ISSN 1067-8212, Russian Journal of Non-Ferrous Metals, 2020, Vol. 61, No. 3, pp. 332–345. © Allerton Press, Inc., 2020.

PRODUCTION PROCESSES AND PROPERTIES OF POWDERS

The Production of AZ31 Alloys by Gas Atomization Method and Its Characteristics

K. M. Em Akra[a], *, M. Akkaş[b], **, M. Boz[a], *, and E. Seabra[c], ******

[a]*Karabük University, Karabük, 78050 Turkey*
[b]*Kastamonu University, Kastamonu, 37150 Turkey*
[c]*Minho University, MEtRICs, 4800-058 Guimarães, Portugal*
**e-mail: kamalakra55@gmail.com*
***e-mail: mehmetakkas@kastamonu.edu.tr*
****e-mail: mboz@karabuk.edu.tr*
*****e-mail: eseabra@dem.uminho.pt*

Received August 24, 2019; revised January 23, 2020; accepted January 29, 2020

Abstract—The aim of this study is to investigate the AZ31 alloy powder production and characterization processes experimentally using the gas atomization method. For this purpose, firstly, the design and production of gas atomization units were done at Karabük University Faculty of Technology Department of Manufacturing Engineering. In this gas atomization unit, the manufacturability of AZ31 powder from magnesium alloys was investigated by the gas atomization method which is one of the production methods by powder metallurgy. The parameters and the literature used in the production of materials similar to the AZ31 alloy are taken into account as producibility parameters. In the gas atomization method, parameters such as nozzle diameter, gas pressure, and temperature must be controlled in order to produce the desired properties in metal powder production. The diameter of the nozzle is crucial because it affects the gas pressure and temperature, the size of the powder, and the shape of the powders. Experimental studies were carried out using 3 different temperatures (790, 820, and 850°C), 4 different nozzle diameters (2, 3, 4, and 5 mm) and 4 different gas pressures (5, 15, 25, and 35 bar). In the molten metal atomization process and in the process of forming a protective gas atmosphere, argon gas was preferred. Scanning electron microscopy (SEM) was used to determine the shape of the AZ31 powders produced, XRD, XRF, and SEM-EDX analyses were used to determine the phases in the internals of the produced powders and percentages of these phases. Laser measurement devices were used for powder size analysis and hardness tests were performed to determine the mechanical properties of the produced powders. The powders produced were pressed into masses at 4 different pressing pressures (300, 400, 500, and 600 MPa). The best sinterability values of the bulked powders and sintering process were performed at 3 different temperatures (500, 550, and 600°C). Density measurements were made after pressing and sintering the powders. As a result of the experimental studies, it was found that the powder size decreased with the increase of the gas pressure but the nozzle diameter, and the powder shape changed to the dripping and the spherical in the ligament and complex form. It has been observed that the temperature has no significant effect on the powder size and shape.

Keywords: gas atomization, AZ31 alloy, magnesium, powder production, powder metallurgy
DOI: 10.3103/S1067821220030074

1. INTRODUCTION

Magnesium alloys have an importance in the defense industry and the transport industry due to their density of 1.74 g/cm^3 along with their lightweight and high specific strength properties [1–6]. Since it has low strength and toughness values without alloying, it is generally used by forming the alloy with other elements. Magnesium also has properties like high thermal conductivity, good electromagnetic protection, high dimensional stability, good absorbing, easy recycling and good workability [7–10]. With these properties, Mg alloys are used in many industries such as automotive, aerospace, computer, sports equipment, and mobile phones. It is also used as an implant material due to its low weight and metabolism compatibility [11–16].

For the last 20 years, metal powder production with gas atomization has been widely used due to properties such as chemical homogeneity and uniform microstructure [17].

Atomization is the process of solidifying the liquid metal with a gas such as air, nitrogen, argon or helium and forming the solidified droplets into powders. In gas atomization, there are processing parameters such

as gas pressure, nozzle diameter, and temperature which affect the powder grain size and distribution. In this study, the effects of atomization variables such as gas pressure, nozzle diameter and metal melting temperature on powder particle size and distribution, powder form and microstructure were investigated [18].

As a result of the literature research, any studies related to the production of AZ31 magnesium alloy powder by gas atomization method could not be found. For this purpose, AZ31 magnesium alloy powder production was studied in order to fill this gap in the literature. In the present experimental work, the powder size distribution of AZ31, the powdered grain shape, the phases of the powders and the concentration of these phases, along with the elemental and chemical composition of the powders and the mechanical strength values of the produced pieces were determined.

2. EXPERIMENTAL

Experimental studies were carried out at the Gas Atomization Unit at Karabük University, Manufacturing Engineering Department of Technology Faculty. The Gas Atomization Unit is shown in Fig. 1, it consists of seven basic parts: Melting furnace, Atomization tower, Nozzle and nozzle holder, Powder collection unit, Gas system, Cyclones, and the Control panel.

Gas-atomized AZ31 powder was produced using a closely matched circular perforated supersonic nozzle system during operation in a gas atomization device. During the atomization work, the liquid was superheated at the AZ31 melting temperature (620°C). The operations performed during the atomization work are listed below. First, the nozzle holder for the test was placed at the bottom of the furnace. The nozzle used in the experiment was placed in the nozzle holder to provide flow between the pot and the nozzle holder. The stainless-steel pot was placed on the nozzle in the furnace. The furnace top cover is closed. A graphite plug having a stainless-steel annular thread system that controls the flow of molten metal when the lid is closed is mounted in a manner to provide a seal for the center of the pot in the furnace. During the metal melting process, argon gas is flown into the furnace at a low pressure (about 2 bar) to protect the molten metal from the onset of oxidation and combustion reactions. About 50 g of AZ31 material in the form of an ingot was used for each test, the AZ31 material was heated to 790 for one hour. The temperature of the melted material was measured by means of two thermocouples that were immersed into the stainless pot and were located outside the pot. Argon gas was given at low pressures within the atomization tower for 15 min before the atomization process to prevent the produced powders from reacting with air. The atomization gas pressure was adjusted to the desired pressure with manometer and gas was sent to the nozzle. It is

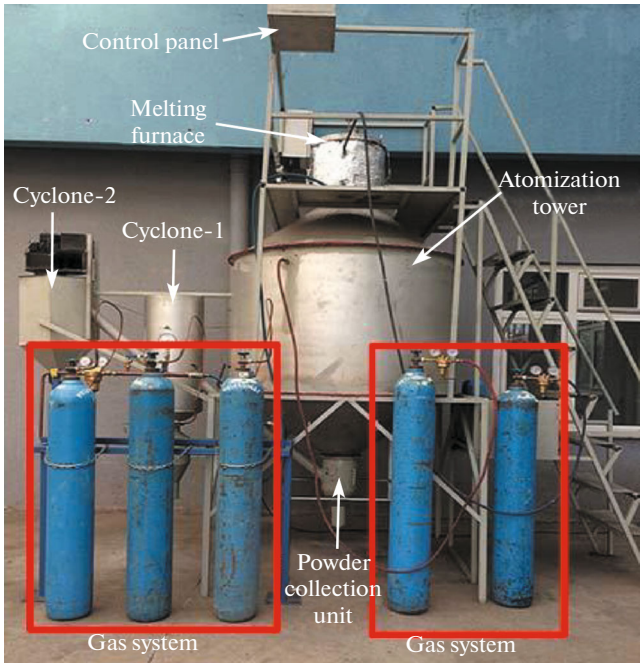

Fig. 1. Gas atomization unit [19].

ensured that the molten AZ31 alloy is flowing and atomized by argon gas by turning up the graphite plug with a worm screw system. After the metal flow was completed, the gas flow was stopped, and the atomization process was completed. Powder collected in the powder collector and cyclones were stocked in desiccators. The powder collector, cyclones and atomization tower were cleaned for the next test.

The atomization parameters of the AZ31 powders produced by the gas atomization method are given in Table 1.

The number of samples was $4 \times 4 \times 3 = 48$ samples. Four variations of nozzles (2, 3, 4, 5 mm), four pressure variations (5, 15, 25, 35) bar, and three temperature variations (790, 820 and 850°C).

Powder size analyses were performed with the Mastersizer 3000 model device in Bartın University Central Research Laboratory. The principle of operation of the device is the red and blue laser light on the sample. The laser light reflected from the sample and broken rays are examined by detectors. The angle and intensity of the scattered light determine the particle size distribution of the sample. Pure water was used as a vector medium during measurements. The scattering angle of the laser light passing through the particle depends on the size of the particle. With low particle size, the scattering angle increases logarithmically. The dispersion angles of the large particles are low, the intensity of the scattered laser light is high. In small particles, the dispersion angle is high, and the intensity of the scattered laser light is low.

Table 1. Powder production parameters

Sample no.	Melting metal temperature, °C	Nozzle diameter, mm	Gas pressure, bar
1, 17, 33	790, 820, 850	2	5
2, 18, 34			15
3, 19, 35			25
4, 20, 36			35
5, 21, 37		3	5
6, 22, 38			15
7, 23, 39			25
8, 24, 40			35
9, 25, 41		4	5
10, 26, 42			15
11, 27, 43			25
12, 28, 44			35
13, 29, 45		5	5
14, 30, 46			15
15, 31, 47			25
16, 32, 48			35

The SEM images and the EDX analysis of the AZ31 alloy powder were obtained from the Carl Zeiss Ultra Plus Gemini Fesem SEM at the Iron and Steel Research Institute of Karabuk University. For the SEM images, the powders were placed on "carbon tape" and covered with gold.

The XRD measurements of the powders were performed with the RIGAKU-Ultima IV model device as seen. XRF measurements were taken with the help of the RIGAKU ZSX Primus II model device. The measurements were carried out at the Karabük University Iron and Steel Research Laboratories. X-ray diffraction (XRD) is a method used to study the crystalline atomic and molecular structure. X-ray Fluorescence (XRF) spectroscopy provides the opportunity to determine the elemental composition.

3. RESULT AND DISCUSSION

In this chapter; different temperatures, different nozzle diameters, different gas pressures, powder size and shape, density, hardness, bending, microstructure, compressibility, and sinterability properties of AZ31 powders are discussed.

The results of the analysis obtained from the Mastersizer 3000 laser size analyzer include D_v (10), D_v (50) D_v (90), specific surface area, D [3, 2], D [4, 3] cumulative percentage values of the produced powders. In addition, the powder size distribution (frequency) and cumulative percentage curves are given.

D_v (10), D_v (50) and D_v (90) dimensions and specific surface areas, changes in atomization temperature, atomization gas pressure and nozzle diameter (as obtained from atomization unit) of powders produced at different temperatures (7790, 820 and 850°C) are given in Table 9.1. According to the results given in Table 9.1, it is seen that powder size decreases with increasing gas pressure and powder size increases with increasing nozzle diameter. It is understood that an increase in atomization temperature from 790 to 850°C resulted in an increase in powder size.

The effect of gas pressure and nozzle diameter on the size of powders produced at different atomization temperatures (790, 820, and 850°C) is given in Fig. 2.

When the results that are given in Fig. 2 are examined, it is seen that for all temperature values, the powder size decreases when the gas pressure is increased, and the powder size increases due to the increase in nozzle diameter. The reason for this is that more energy is transferred to molten metal due to the increased gas pressure and increased atomization effect which resulted in smaller powder production. The reason for the decrease of the powder size with the decrease of the nozzle diameter is interpreted as the increase of the liquid metal flowing from the nozzle and the decrease of the energy per unit area on the molten metal.

It is known that gas pressure has a significant effect on powder size and shape in powder production by gas atomization method. In the experimental studies, the highest gas pressure value was taken as 35 bar. Above the highest pressure value, the powder production could not be performed due to the reverse effect (positive pressure) of the atomization gas on the nozzle which causes a blockage to the flow of the molten metal. A temperature of 850°C, nozzle diameter of 2 mm and the smallest average powder size at different gas pressures were obtained at a nozzle diameter of 2 mm and a gas pressure of 35 bar. While this value is 79.1 μm at 820°C atomization temperature, the smallest value was with 46 μm at 790°C atomization temperature. In general, 10% of the powders produced for these variables are less than 21.6 μm, while 90% are less than 252 μm. It was determined that at least 10% of the produced powders consisted of powders below 10 μm. However, since these powders were sprayed into atomization towers and cyclones as well as into containers where the powders were stored, the intake of these powders was not possible.

As a result of the experiments carried out in the production of AZ31 powder by gas atomization method, the effect of gas pressure was clearly seen. It is also evident from the SEM images given in Fig. 3 that the particle size of the produced powders decreased when the gas pressure increased.

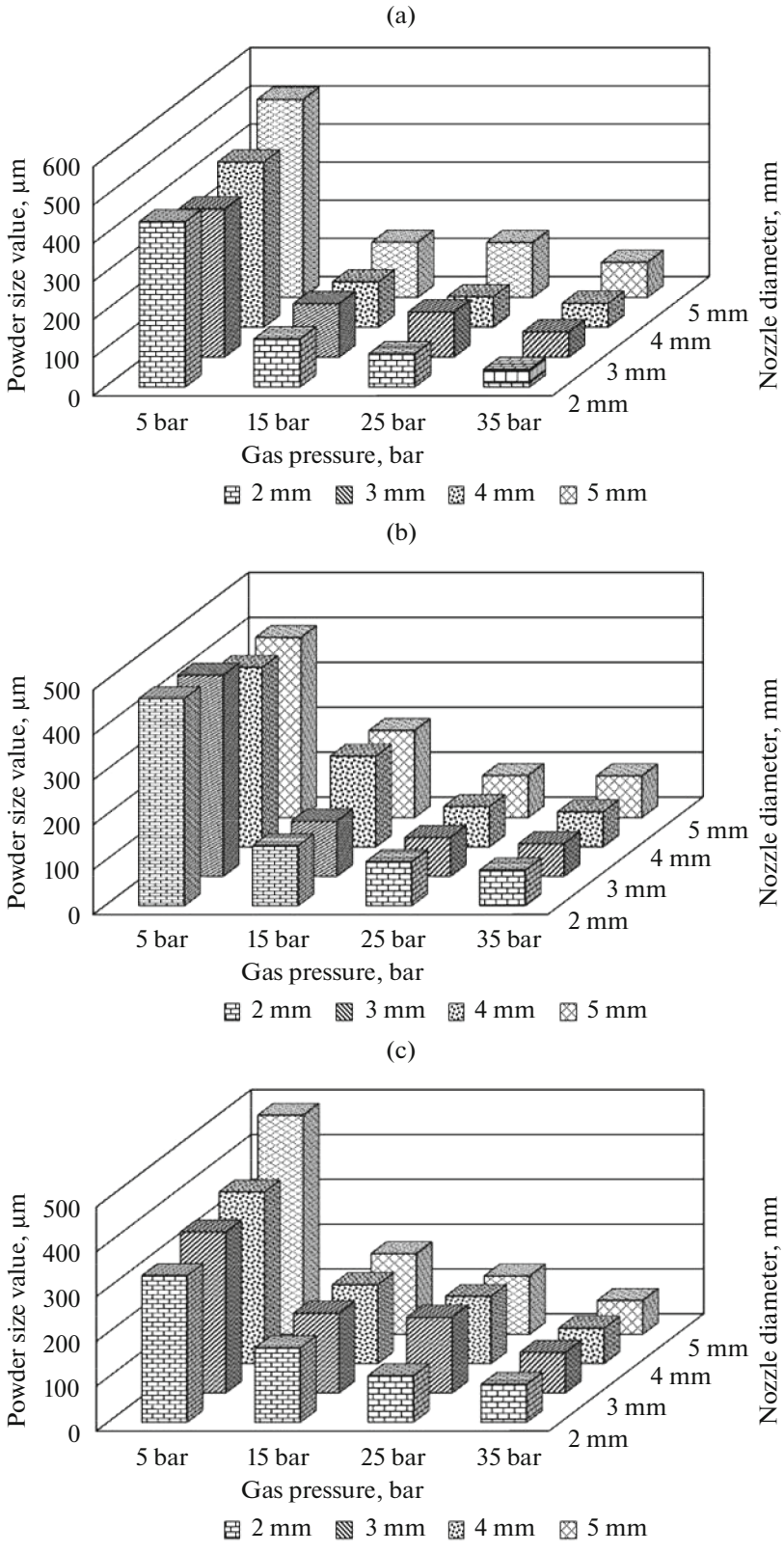

Fig. 2. Effect of atomization gas pressure and nozzle diameter on powder size values of AZ31 powders produced. (a) 790, (b) 820, and (c) 850°C.

Table 2. Particle size of AZ31 powders

Atomization temperature, °C	Nozzle diameter, mm	Gas pressure, bar	D_v (10), μm	D_v (50), μm	D_v (90), μm	Specific surface area, m^2/kg
790	2	5	174	433	878	18.46
		15	73.9	126	441	43.19
		25	36	86.6	267	84.58
		35	18.1	46	99.2	186.7
	3	5	136	388	847	22.09
		15	53.9	140	367	58.98
		25	44.7	118	330	68.51
		35	28.1	66.1	146	117.8
	4	5	173	433	870	19.05
		15	52.2	119	256	64.67
		25	26.5	62.6	131	124.7
		35	35.4	80.2	235	90.38
	5	5	227	519	1070	14.73
		15	56.6	145	427	54.73
		25	54	144	402	57.31
		35	28.3	92.0	203	113.1
820	2	5	176	461	1050	17.82
		15	41.8	133	287	70.73
		25	25.9	98	211	119.5
		35	31.2	79.1	201	101.6
	3	5	212	448	926	15.95
		15	47.3	123	353	65.24
		25	19.7	86.6	223	151.7
		35	24.2	72.8	195	143.7
	4	5	93.3	400	1050	27.95
		15	67.9	202	586	43.01
		25	45.3	90.1	392	64.17
		35	44.2	78	484	62.71
	5	5	65.1	401	773	41.97
		15	68.6	194	526	44.05
		25	24.5	93.8	263	127.8
		35	32	92.8	255	94.98
850	2	5	167	327	906	19.15
		15	57.5	166	450	52.53
		25	22	104	378	169.2
		35	21.6	84.6	252	143.7
	3	5	79.2	359	911	32.52
		15	39.8	178	302	72.88
		25	65.8	169	453	47.38
		35	35	90.3	231	93.56
	4	5	100	383	984	27.89
		15	56.9	176	367	56.51
		25	25.8	150	230	124.6
		35	26.7	78.8	232	124.5
	5	5	160	489	864	20.04
		15	67.6	180	441	46.75
		25	40.9	130	416	72.65
		35	19.3	75.6	177	167.9

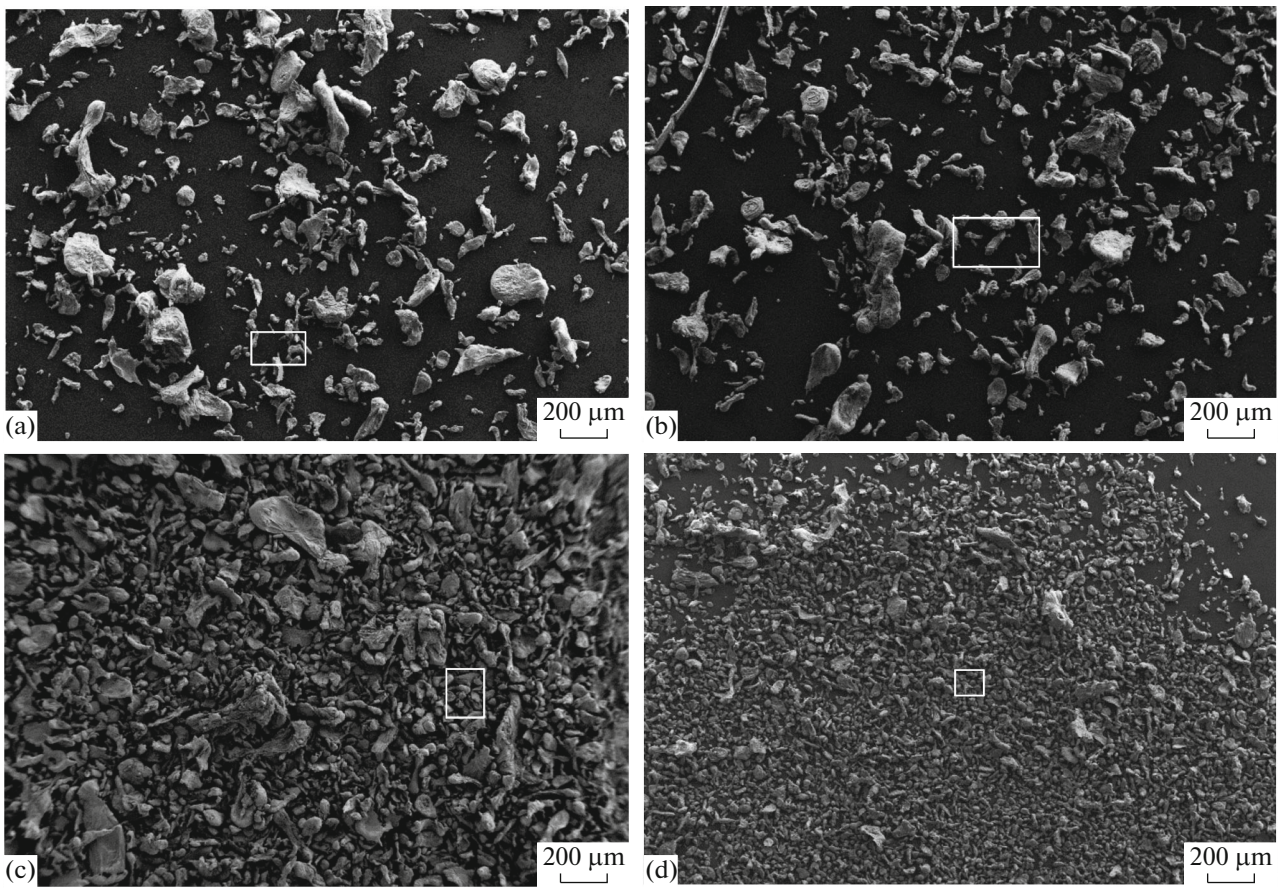

Fig. 3. SEM images of powders produced at 2 mm nozzle diameter, 790°C (100×) at different gas pressures (a) 5, (b) 15, (c) 25, and (d) 35 bar.

In the literature studies on this subject, it has been stated that the powder size decreases due to the increase in gas pressure [19–22]. It can be seen in Fig. 3 that the average powder size is reduced due to the increase in gas pressure and the results obtained from this study are consistent with the literature. On the other hand, it is understood from Fig. 4 that the powders produced are generally in the form of ligaments, droplets, rods, flakes, and spheres.

In the SEM images given in Fig. 5, it is seen that the powder shape changes from ligament, rod, and complex shape to flake, droplet and spherical due to the increase in gas pressure. It is seen that powder produced especially at 35 bar gas pressure and shrinks its shape significantly into drip and spherical shapes as is seen in Fig. 5. Figure 5a shows that a small proportion of the powders are spherical. The most important reason for this is thought to be the low atomization gas pressure and the insufficiency of the atomization tower. The powder particles solidified by hitting the bottom of the atomization tower before they had time to attain a spherical shape.

SEM images of AZ31 powders produced at an atomization temperature of 820°C, nozzle diameter of 2 mm and atomization gas pressures of 5, 15, 25, and 35 bar are given in Fig. 5. Figure 6 shows the change in the shape and size of the powder produced due to the increase in nozzle diameter.

The SEM images given in Fig. 7 show that the snow-white areas on the surfaces of the powders are oxide (visible from the EDX analysis in Fig. 7) and the amount of oxide formed on the surface increases depending on the gas pressure. The increase in the gas pressure and the increase in the amount of oxide formed on the surface of the powder is thought to be due to the fact that argon gas blown for atomization is not pure and air circulation is intense. In addition, when the surfaces are carefully examined, it can be realized that a grain of powder (as in solidification) is composed of sub-grains and that the sub-grains shrink with increasing gas pressure. The reason for this can be interpreted as the nucleation of the sub-grains due to the solidification rate, as well as the solidification of the liquid metal, depending on the cooling rate and the structure to be composed of smaller particles. On the other hand, it is understood from the SEM images that the increased gas pressure increases the pressure on the unit surface and because of the faster cooling of the surface, a denser surface is formed.

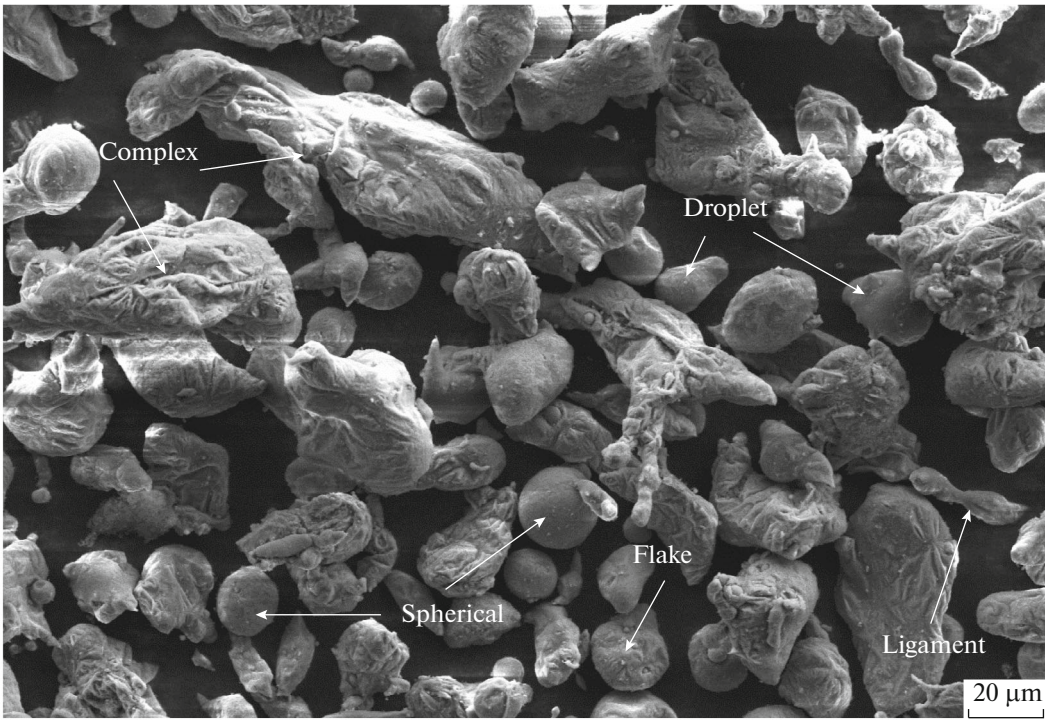

Fig. 4. General SEM view of AZ31 powder produced at an atomization temperature of 790°C.

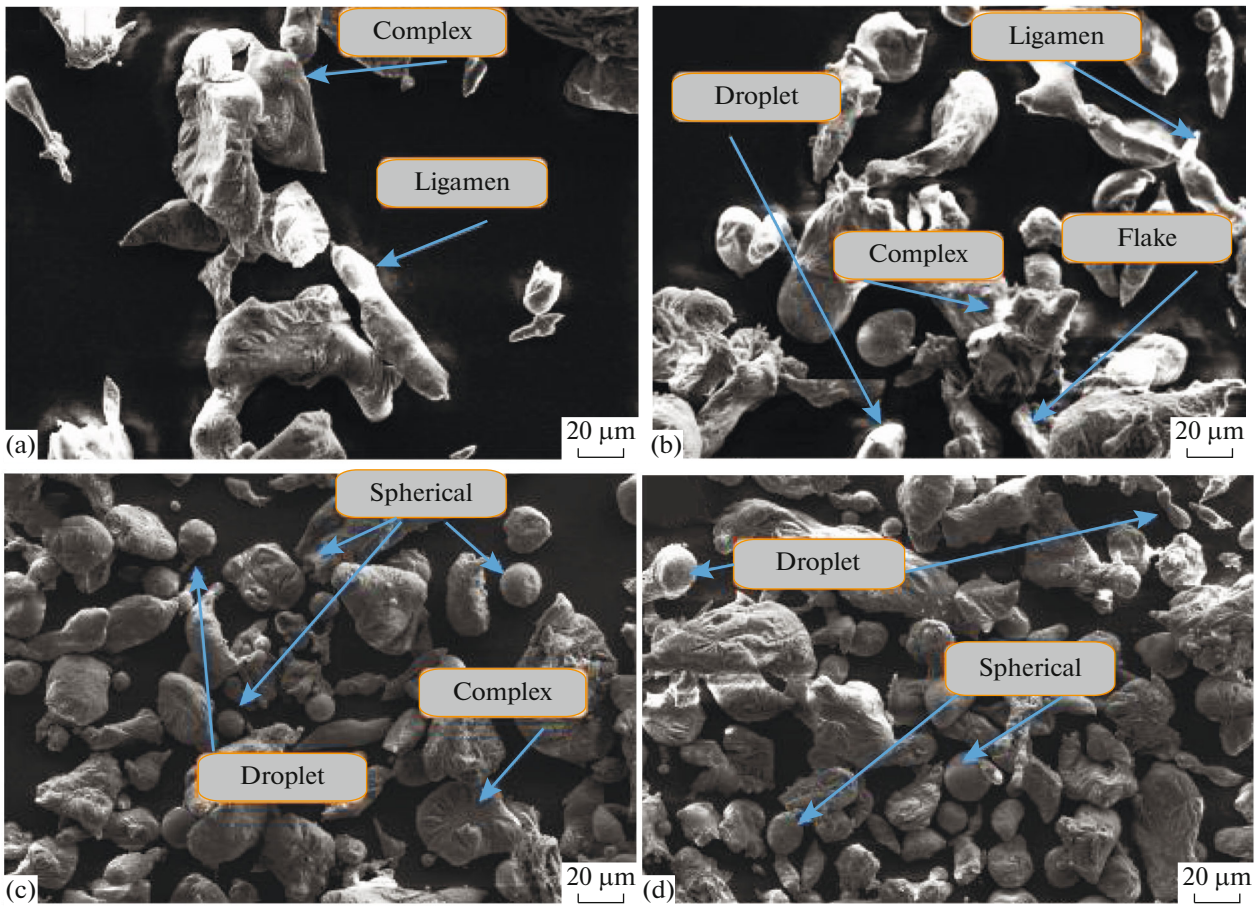

Fig. 5. SEM images of the powders produced at 2 mm, 790°C (1000×) at different gas pressures (a) 5, (b) 15, (c) 25, and (d) 35 bar.

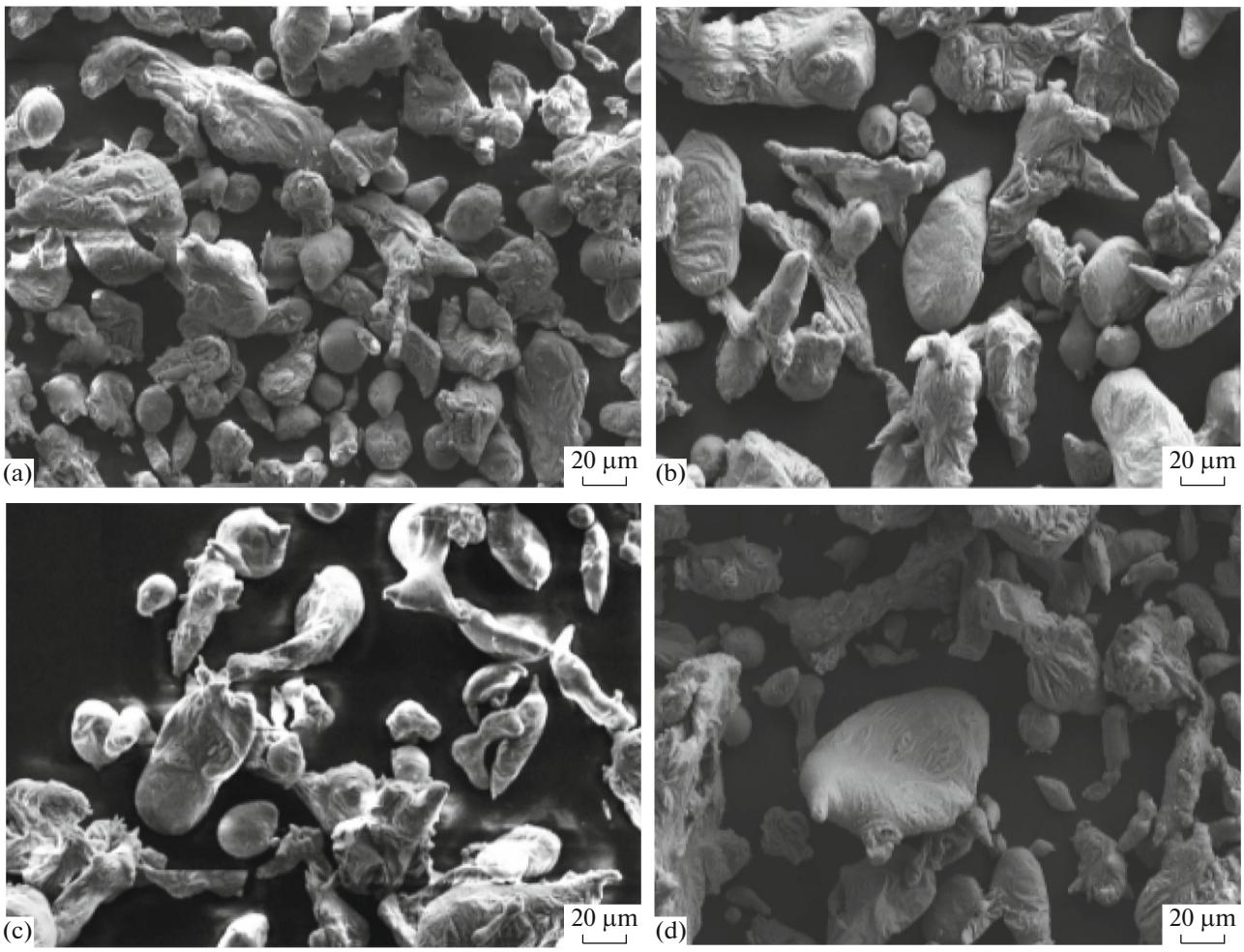

Fig. 6. SEM images of AZ31 alloy powders produced at 790°C, 35 bar gas pressure, and different nozzle diameters. (a) 2, (b) 3, (c) 4, and (d) 5 mm.

In addition, it is known that nozzle diameter has a significant effect on powder size and shape as a production parameter in powder production by gas atomization method. It is clear from the SEM images given in Fig. 6 that the particle size of the produced powders increases when the nozzle diameter is increased. In addition, powders produced with small nozzle diameters are mostly spherical, droplet, and flake, whereas powders produced with nozzle diameters of 4 and 5 mm generally appear to be ligaments, pulses, rods, and complex shapes. The reason that the powders are coarse and complex in larger nozzle diameters is since more liquid metal per unit time passes through the nozzle and insufficient atomization of gas.

In Fig. 7, the SEM-EDX analysis is obtained from 2 different points from the powder produced at 850°C temperature, 4 mm nozzle diameter and 35 bar gas pressure. In the microstructure α-Mg main matrix phase, Al, Si, Zn, and Oxygen are observed.

Figure 8 shows the XRD result of AZ31 alloy powder. When the XRD result is analyzed, the α (Mg main matrix) phase, β phase $Mg_{17}Al_{12}$ and MgO are seen in the structure. $Mg_{17}Al_{12}$ precipitates are known to provide mechanical reinforcement for the AZ31 alloy at the expense of ductility [23]. The mechanical behavior of the alloy depends on the amount, morphology and size of the precipitate. In the AZ31 alloy, strength and creep resistance decrease due to the softening of the $Mg_{17}Al_{12}$ phase above 120°C [24]. AZ31 consists of hexagonal tight package α-Mg and eutectic α + β (β phase, called body-centered cubic β-$Mg_{17}Al_{12}$ phase) phases [25].

The XRD results given in Fig. 8 show that powders produced at different gas pressures by gas atomization have no effect on the chemical composition of the powder.

Table 3. Chemical composition of AZ31 alloy

Material	Mg	Al	Zn	Mn
Content, %	95.71	2.77	1.10	0.40

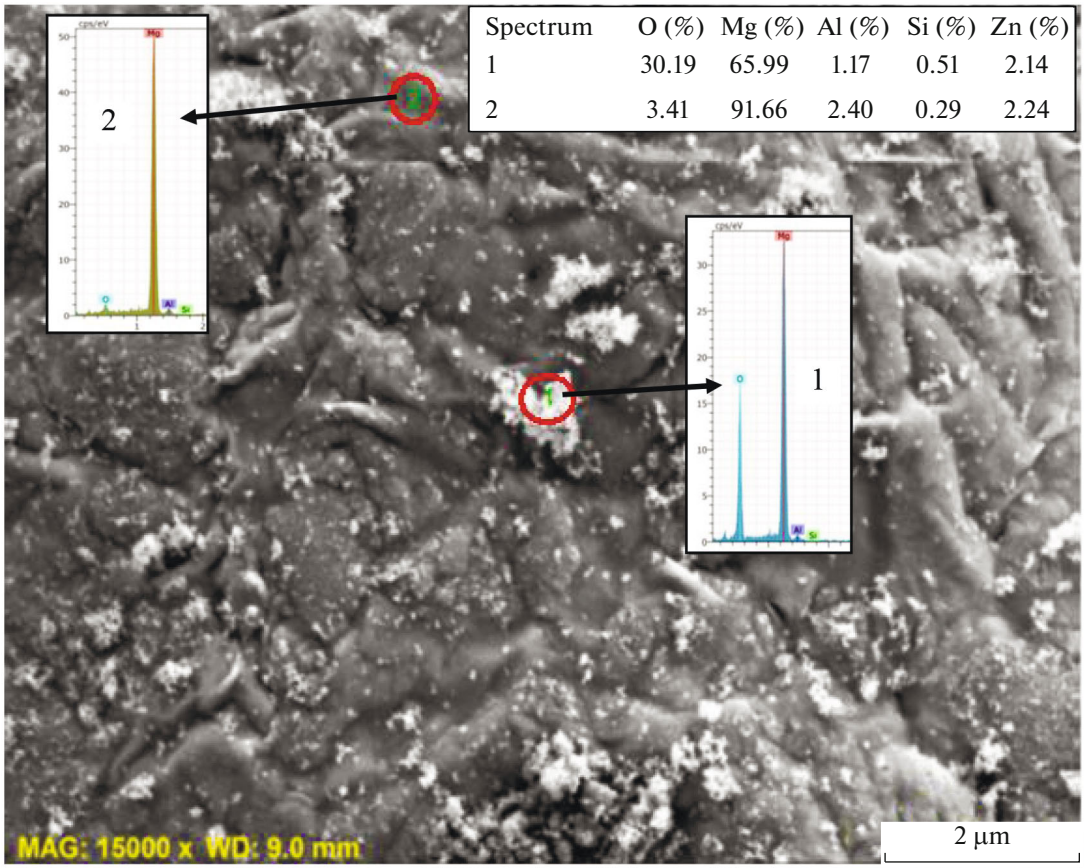

Fig. 7. EDS analysis of AZ31 powders produced at 850°C, 4 mm nozzle diameter and 35 bar pressure.

Chemical composition analysis of AZ31 material provided as ingot is given in Table 3. In addition, XRF chemical analysis results of AZ31 alloy powder produced by the gas atomization method are given in Table 4.

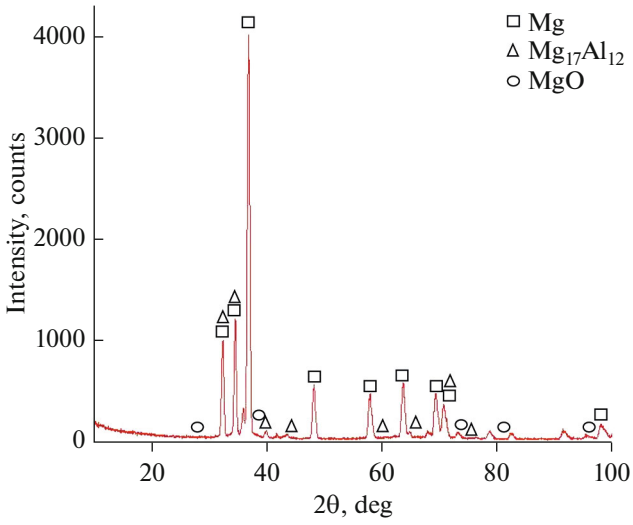

Fig. 8. XRD pattern of magnesium alloy AZ31.

When Tables 3 and 4 were examined, it was found that the chemical composition of the AZ31 material, which was pulverized by gas atomization, was almost the same. When Tables 3 and 4 are compared, it is observed that very little Mg is decreased. It is understood from Fig. 7 that the reduction in magnesium is due to oxidation during melting or atomization. Furthermore, the fact that the chemical composition is changed by atomization which shows that the production of powder by the gas atomization system is important.

3.1. Sinterability of Produced Powders and Parts Production

The density values of the samples which are massed at different pressing pressures depending on the pressing pressure are given in Table 5.

When Table 5 is examined, it is seen that pressing (600 MPa) has no effect on the relative density of the samples. Akkaş et al. [20, 26], in their work on the pressing and sintering of AZ91 powder produced by gas atomization, stated that the relative density values of the samples increased due to the increase of pressing pressure and sintering temperature. They stressed

that the raw density of the sample at 300 MPa pressing pressure was 82.73%, whereas this value was 92.4% at 600 MPa pressing pressure [20, 26]. However, in this study, it was observed that there was no change in the relative density of samples under pressure of 400 and 600 MPa. The reason for this is thought to be caused by the reduction of Aluminum powder with a face-centered-cubic crystal lattice structure which is easier to deform in the AZ31 alloy. Therefore, Table 5 shows that the highest cold pressing pressure of AZ31 alloy powder is 600 MPa. The density values of 3 different pressing pressures were found to be 91 MPa on average. For this purpose, pressed samples at 600 MPa pressure will be used in all subsequent sintering and other processes.

For this purpose, powders produced at a temperature of 850°C and a nozzle diameter of 2 mm, pressed at 600 MPa, and the pellets massed were subjected to sintering in an atmosphere-controlled furnace at three different temperatures (500, 550 and 600°C) for one hour.

In order to determine the optimum sintering temperatures of the materials pressed at 600 MPa pressure, the parameters given in Table 6 were applied.

The samples formed into ingots were sintered at three different temperatures (500, 550, and 600°C). The density values of sintered AZ31 alloys after sintering were determined. The density values of the samples after mass sintering are given in Table 7.

When the density results are examined in Table 7, the average relative densities of the samples increased with sintering. However, it is seen that the increase in sintering temperature does not have much effect on the densities of the samples. The density values of the powders which were massed at different pressures and then sintered at different temperatures were determined. Density values before and after sintering were determined separately for each sample. The average density values for each pressure applied were calculated for the density values which are determined separately for each sample. The relative densities of the sample pressed at a pressure of 600 MPa before sintering are given in Fig. 9.

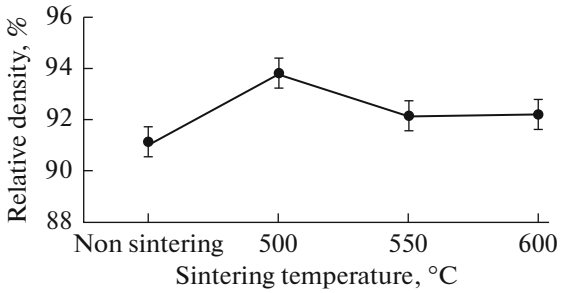

Fig. 9. Density values of samples.

The relative density of the samples increased with sintering is shown in Table 7. While the relative density of the sample at 600 MPa pressing pressure was 91.23% before sintering, the relative density value of the same sample with sintering at 500°C was recorded as 93.78%. Sintering at 550 and 600°C results in a slight decrease in relative density values. It is known that with sintering, the density increases due to the disappearance of small pores in the material and the grain boundaries approaching each other. However, after the sintering temperature of 500°C, the relative density of the sample decreases.

Table 4. Chemical (XRF) analysis of produced AZ31 powders

Material	Mg	Al	Zn	Mn	Si
Content, %	94.71	2.75	1.62	0.61	0.22

Table 5. Before sintering density results of AZ31 alloys

No.	Pressing, MPa	Weight, g	Length, cm	Width, cm	Thickness, cm	Volume, cm^3	Density, g/cm^3	Relative density, %	Average relative density, %
1	600	4.683	3.2	1.3	0.685	2.8496	1.6433	91.2993	91.123
2		4.71	3.2	1.3	0.70	2.912	1.6174	89.8580	
3		4.902	3.2	1.3	0.701	2.9536	1.6596	92.2038	
4		4.702	3.2	1.3	0.69	2.8704	1.6380	91.0055	91.127
5		4.669	3.2	1.3	0.69	2.8704	1.6266	90.3668	
6		4.685	3.2	1.3	0.68	2.8288	1.6561	92.0099	
7		4.709	3.2	1.3	0.7	2.912	1.6171	89.8389	91.014
8		4.683	3.2	1.3	0.68	2.8288	1.6554	91.9706	
9		4.691	3.2	1.3	0.71	2.9536	1.5882	89.2350	

Table 6. Sintering parameters of the samples

Sample no.	Pressing value, MPa	Sintering temperature, °C
1	600	500
2		550
3		600

Changes in grain boundary thickness and increase of sintering temperature of $Mg_{17}Al_{12}$ which causes pore growth are given in Figs. 10–12.

When the SEM image given in Fig. 10 is examined, it is seen that $Mg_{17}Al_{12}$ intermetallic phase is homogeneously distributed in the structure in the sintered sample at 500°C. However, in the samples sintered at the temperatures of 550 and 600°C, SEM images in Figs. 11 and 12 show that the $Mg_{17}Al_{12}$ intermetallic phase is not homogeneously deposited at the grain boundaries and even becomes larger. The reason for the growth of the $Mg_{17}Al_{12}$ intermetallic phase and the grain boundaries is thought to be that a portion of the $Mg_{17}Al_{12}$ intermetallic phase dissolves in the α-Mg phase and that some of it grows by combining with the $Mg_{17}Al_{12}$ intermetallic phase formed at the grain boundaries. In addition, it is thought that the intermetallic phase of $Mg_{17}Al_{12}$, which increases at high sintering temperatures (500 and 600°C), settles at the grain boundaries, preventing the grain boundaries from approaching each other and causing the pores to decrease. As a result, as shown in Fig. 9, it has caused a decrease in density due to the increase in sintering temperature.

SEM-EDS analysis of the microstructure of the α-Mg matrix as well as along the grain boundary β ($Mg_{17}Al_{12}$) phase and a fine phase in the grain boundary α + β eutectic was observed (Figs. 10–12). On the other hand, when the EDS analysis of the point encoded by the number 2 given in the SEM image in Fig. 10 is examined, a very intensive oxygen content is seen. Oxygen on the surface of the sintered samples is thought to occur both during powder production and during sintering.

The microhardness tests were performed to determine the effect of sintering temperature on the hardness of the samples produced at pressing pressures 600 MPa and different sintering temperatures (500, 550, and 600°C). The hardness tests were performed under 500 gf ($HV_{0.5}$) and 15 s of retention time. The hardness values were determined by calculating the average of 3 hardness values of each sample. Hardness results are given in Table 8.

When the hardness results given in Table 8 are examined, the highest hardness value was 54.86 $HV_{0,5}$ at the same 600 MPa pressing pressure and 500°C sintering temperature. At the same 600 MPa pressing pressure, 600°C sintering temperature produced the lowest hardness value which was measured to be 53.8 $HV_{0,5}$. The decrease in the hardness values due to the increase in the sintering temperature can be explained by the SEM images in Figs. 10–12. When the surface images of the sintered samples in Figs. 10–12 are examined, it is seen that the $Mg_{17}Al_{12}$ precipitates are distributed to the whole surface homogeneously in the sample produced at 500°C, whereas in the sample produced at 600°C $Mg_{17}Al_{12}$ is located at the grain boundaries. Hence, as the hardness test measurements of the samples are made homogeneously from all surfaces decrease due to the increased sintering temperature [18, 20, 27].

4. GENERAL RESULTS

In this study on the characterization of AZ31 powder produced by the gas atomization method under different parameters were carried out, the results obtained from this study are summarized below.

Table 7. Density results of sintered AZ31 alloys

No.	Sintering temp., °C	Weight, g	*L*, cm	*W*, cm	*T*, cm	Volume, cm^3	Density, g/cm^3	Relative density, %	Average relative density, %
1	500	4.486	3.170	1.280	0.66	2.67801	1.6751	93.0622	93.785
2		4.666	3.185	1.290	0.67	2.75279	1.6950	94.1669	
3		4.580	3.175	1.290	0.66	2.70319	1.6942	94.1272	
4	550	4.198	3.150	1.260	0.64	2.54016	1.6526	91.8139	92.157
5		4.209	3.150	1.270	0.63	2.52031	1.6703	92.7944	
6		4.166	3.135	1.250	0.65	2.54718	1.6355	91.8627	
7	600	4.373	3.180	1.270	0.64	2.58470	1.6918	93.9931	92.241
8		3.816	3.155	1.270	0.58	2.32397	1.6420	91.2230	
9		4.491	3.190	1.295	0.66	2.72649	1.6471	91.5094	

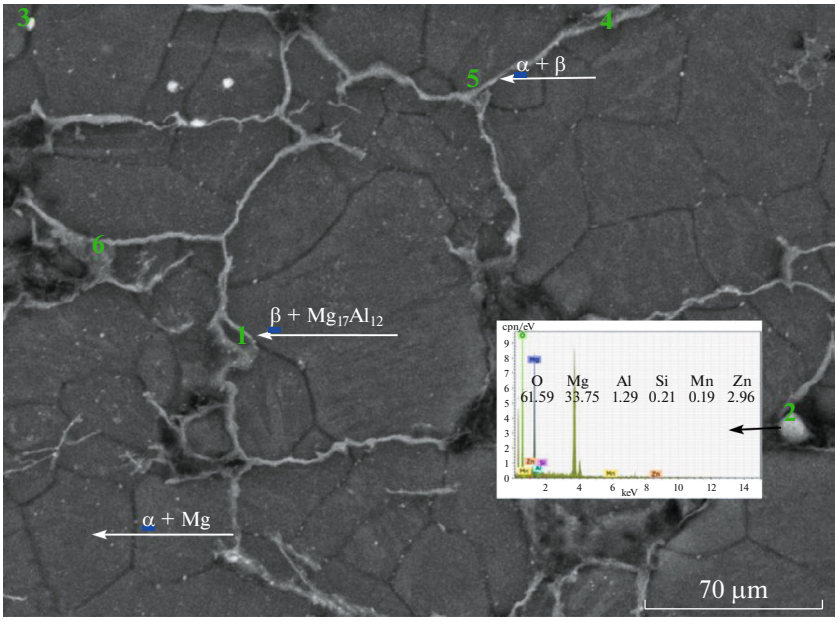

Fig. 10. SEM images and EDX analysis after sintering at 500°C.

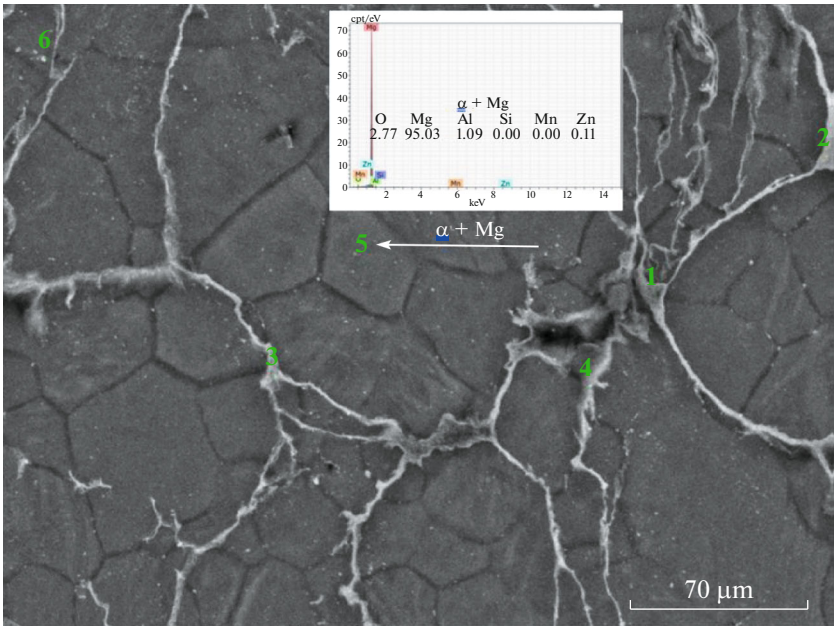

Fig. 11. SEM images and EDX analysis after sintering at 550°C.

• It is understood that the temperature of the liquid metal in the production of powder by gas atomization method has little effect on the size, distribution, shape and surface appearance of the powders.

• When the nozzle diameter was decreased and gas pressure was increased, it was observed that the powder size decreased and the powder shape changed from complex, ligament, pulse and rod-like structure to dripping and spherical. In addition, since the pressure increase provides for transferring more energy to the melt, the powders produced have a smaller average powder size. In the production of gas atomized magnesium alloy AZ31 powder, the smallest powder size was measured to be 46 μm under the condition of 790°C, 2 mm nozzle diameter and at 35 bar pressure.

• During the atomization, different formations of satellites were observed on the surfaces due to the clashes between droplets and powders. Furthermore,

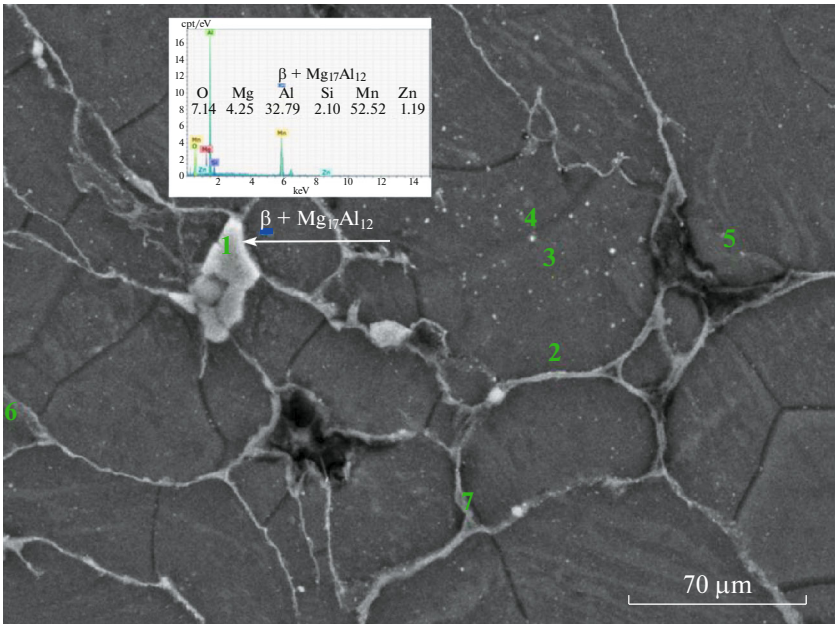

Fig. 12. SEM images and EDX analysis after sintering at 600°C.

it was observed that the surfaces of the powder vary depending on the gas pressure and they have dendritic and cellular shapes.

• At the end of XRF, it was seen that the chemical composition of AZ31 powder and ingot material had almost the same proportion of elements.

• As a result of the XRD analysis, microphase α (Mg main matrix) and phase β (Mg17Al12) was observed.

• Sintered samples at three different temperatures (500, 550, and 600°C) were examined and a decrease of their relative density after sintering was seen. The sample having the highest relative density value after the sintering process was measured to be 93.785% which was compressed at 600 MPa pressure and sintered at 500°C.

• After sintering, XRD analysis results showed that α-Mg, β ($Mg_{17}Al_{12}$) and α + β phases were present in the structure. However, XRD analysis before sintering clearly showed Mg peaks, while the XRD analysis after sintering showed a slight decrease in the degree of Mg peaks. In addition, it was seen in XRD analysis that the $Mg1_7Al_{12}$ phase became clearer to observe due to the increased sintering temperature. After sintering, it was determined that the decrease in Mg phase was caused by precipitation in the material.

Table 8. Hardness values after sintering

Pressure, MPa	Sintering temp., °C	Average value ($HV_{0.5}$)
600	500	54.86
	550	54.33
	600	53.80

• In the SEM images, the ductile fractures of the sintered materials were observed at high sintering temperatures. In lower sintering temperature values, fractures were observed at grain boundaries. It is believed that internal energies increase the deformation of particles and increase their size during sintering.

• The hardness values of the samples decreased due to the increase in sintering temperature. The decrease in these hardness values is thought to be caused by the formation of a brittle structure due to sintering temperature and rapid solidification during atomization. In the samples sintered at low temperatures, $Mg_{17}Al_{12}$ was distributed to the entire surface homogeneously, whereas, in the sample produced at 600°C, Mg17Al12 was deposited on the grain boundaries. Hence, as the hardness measurements of the samples were made homogeneously from all surfaces, the hardness measurement results decreased due to the increased sintering temperature. The highest hardness values of the massed samples were measured to be 54.86 $HV_{0.5}$ at 600 MPa pressing pressure and 500°C sintering temperature.

CONFLICT OF INTEREST

The authors declare to have no conflict of interest.

REFERENCES

1. Mordike, B.L. and Ebert, T., Magnesium properties applications potential, *Mater. Sci. Eng., A,* 2001, vol. 302, pp. 37–45.
2. Benedyk, J.J., Magnesium challenges aluminum dominance as the light metal of choice in automotive markets, *Light Met. Age,* 2004, vol. 62, no. 8, p. 5.
3. *ASM Metals Handbook,* vol. 14: *Forming and Forging,* West Conshohocken, PA: American Society for Testing and Materials, 1988, pp. 791–804.
4. Li, Y., and Zhang, Y., Light-weight and flexible high-entropy alloys, in *High Entropy Alloys*, Intechopen, 2019.
5. Niu, Y., Song, Z., Le, Q., Hou, J., and Ning, F., Excellent mechanical properties obtained by low temperature extrusion based on Mg–2Zn–1Al–0.2Mn–0.2Ca–0.2Gd alloy, *J. Alloys Compd.,* 2019. https://doi.org/10.1016/j.jallcom.2019.05.297
6. Rajan, A.V., Sundaram, C.M., and Rajesh, A.V., Mechanical and morphological investigation of bio-degradable magnesium AZ31 alloy for an orthopedic application, *Mater. Today: Proc.,* 2019; Rajan, A.V., Sundaram, C.M., and Rajesh, A.V., Mechanical and morphological investigation of bio-degradable magnesium AZ31 alloy for an orthopedic application, *Mater. Today: Proc.,* 2020, vol. 21, pp. 272–277.
7. Fredrich, H. and Schumann, S., Research for a new age of magnesium in the automotive industry, *J. Mater. Process. Technol.,* 2001, vol. 117, pp. 276–280
8. Furuya, H., Kogiso, N., Matunaga, S., and Senda, K., Applications of magnesium alloys for aerospace structure systems, *Mater. Sci. Forum,* 2001, vols. 350–351, pp. 341–351.
9. Froes, F.H., Eliezer, D., and Aghion, E., The science, technology, and applications of magnesium, *J. Mater. Process. Technol.,* 1998, vol. 50, no. 9, pp. 30–34.
10. Vignesh, R.V., and Padmanaban, R., Forecasting tribological properties of wrought AZ91D magnesium alloy using soft computing model, *Russ. J. Non-Ferrous Met.,* 2018, vol. 59, no. 2, pp. 135–141.
11. Gray, J. and Luan, B., Protective coatings on magnesium and its alloys-a critical review, *J. Alloys Compd.,* 2002, vol. 336, nos. 1–2, pp. 88–113.
12. Kaya, R.A., Çavuşoğlu, H., Tanık, C., Kaya, A.A., Duygulu, Ö., Mutlu, Z., Zengin, E., and Aydın, Y., The effects of magnesium particles on posterolateral spinal fusion: an experimental in vivo study in a sheep model, *J. Neurosurg.: Spine,* 2007, vol. 6, pp. 141–149.
13. Duygulu, O., Kaya, R.A., Oktay, G., and Kaya, A.A., Investigation on the potential of magnesium alloy AZ31 as a bone implant, *Mater. Sci. Forum,* 2007, vols. 546–549, pp. 421–424.
14. Duygulu, O., Kaya, R.A., Oktay, G., Berk, C., and Kaya, A.A., Can magnesium alloys be used as implants?- SEM examinations from an in vivo study, *Proc. 16th Int. Microscopy Conference,* Sapporo, 2006.
15. Kaya, A.A., Future of magnesium: applications in transportation and bone surgery, *Proc. 10th Int. Symposium on Advanced Materials (ISAM-2007)*, Islamabad, 2007.
16. Kaya, A.A., Kaya, R.A., Witte, F., and Duygulu, Ö., Useful corrosion- potential of magnesium alloys as implants, *Proc. Int. Corrosion Engineering Conference,* Seoul, 2007.
17. Lagutkin, S., Achelis, L., Sheikhaliev, S., Uhlenwinkel, V., and Srivastava, V., Atomization process for metal powder, *Mater. Sci. Eng., A,* 2004, vol. 383, no. 1, pp. 1–6.
18. Ünal, R., *Gaz atomizasyonu ile metal tozu üretimi değişkenlerinin araştırılması, Yüksek Lisans Tezi,* Ankara: Gazi Üniv., 1995.
19. Akkaş, M., Çetin, T., and Boz, M., The effect of gas pressure on powder size and morphology in the production of AZ91 powder by gas atomization method, *Arch. Metall. Mater.,* 2018, vol. 63, no. 4, pp. 1587–1594.
20. Akkaş, M. and Boz, M., Investigation of the compressibility and sinterabilty of AZ91 powder production and particle production by gas atomization method, *J. Magnesium Alloys,* 2019, vol. 7, no. 3, pp. 400–413.
21. Uslan, İ. and Küçükarslan, S., Kalay tozu üretimine gaz atomizasyonu parametrelerinin etkisinin incelenmesi, *Gazi Üniv. Mühendislik Mim. Fak. Derg.,* 2010, vol. 25, no. 1, pp. 1–8.
22. Clyne, T.W., Ricks, R.A., and Goodhew, P.J., The production of rapidly - solidified aluminium powder by ultrasonic gas atomization. Part I: Heat and fluid flow, *Int. J. Rapid Solidif.,* 1984, vol. 1, pp. 59–80.
23. Daloz, D. and Michot, G., Influence of the consolidation step on the mechanical properties of rapidly solidified Mg–Al–Zn alloys, *Int. J. Rapid Solidif.,* 1996, vol. 9, pp. 289–304.
24. Rajan, T.P.D., Jayakumar, E., and Pai, B.C., Developments in solidification processing of functionally graded aluminium alloys and composites by centrifugal casting technique, *Trans. Indian Inst. Met.,* 2012, vol. 65, no. 6, pp. 531–537.
25. Jafarzadeh, A., Ahmadi, T., Dehaghani, M.T., and Mohemi, K., Synthesis, corrosion and bioactivity evaluation of gelatin/silicon and magnesium Co-doped fluorapatite nanocomposite coating applied on AZ31 Mg alloy, *Russ. J. Non-Ferrous Met.,* 2018, vol. 59, no. 4, pp. 458–464.
26. Çetin, T., Akkaş, M., and Boz, M., Investigation of the effect of gas pressure on powder characterization of AM60 magnesium alloy powder produced by gas atomization method, *J. Fac. Eng. Archit. Gazi Univ.*, 2020, vol. 35, no. 2, pp. 967–977.
27. Hu, H.J., Fan, J.Z., Zhai, Z.Y., Wang, H., Li, Y.Y., and Gong, X.B., Physical fields evolution and microstructures for compound extrusion of AZ31 magnesium alloy, *Russ. J. Non-Ferrous Met.,* 2014, vol. 55, no. 3, pp. 254–262.